Surface Crystallization of Liquid Au–Si and Its Impact on Catalysis

Federico Panciera,* Jerry Tersoff, Andrew D. Gamalski, Mark C. Reuter, Dmitri Zakharov, Eric A. Stach, Stephan Hofmann, and Frances M. Ross*

In situ transmission electron microscopy reveals that an atomically thin crystalline phase at the surface of liquid Au–Si is stable over an unexpectedly wide range of conditions. By measuring the surface structure as a function of liquid temperature and composition, a simple thermodynamic model is developed to explain the stability of the ordered phase. The presence of surface ordering plays a key role in the pathway by which the Au–Si eutectic solidifies and also dramatically affects the catalytic properties of the liquid, explaining the anomalously slow growth kinetics of Si nanowires at low temperature. A strategy to control the presence of the surface phase is discussed, using it as a tool in designing strategies for nanostructure growth.

Understanding the phenomena that occur at the surface of liquid metals is critical for technological applications ranging from catalysis to soldering to crystal growth. However, liquid-metal surfaces can be complex and exhibit puzzling phenomena. Liquid-metal alloys commonly exhibit Gibbs adsorption effects, where the surface layer is enriched in the element with the lower surface tension.[1,2] Density oscillations are also commonly observed at the surface[3,4] and the surface may even be ordered.[1,2,5–7] Au–Si, a liquid metal, is unique in forming a 2D crystalline compound at its surface, with a

fixed atomic-scale thickness, over a range of temperature. While this layer has not been imaged directly, diffraction studies have established that an ordered bilayer (the low-temperature (LT) phase) exists up to 12 °C above the eutectic temperature.[2,8] (A higher temperature phase has also been detected, although its properties are less clear.[9,10]) At present there is no straightforward explanation for this unique behavior. Ordered surface phases have been explained by surface prefreezing,[11] a phenomenon that is analogous to the well-known surface premelting. However, an ordered prefreezing layer is expected to be present only very near the transition temperature and to have a thickness that diverges as the temperature approaches the transition temperature, both of which are inconsistent with the behavior of Au–Si. The ordered surface phase in Au–Si also cannot be explained as a solute coming out of solution and wetting the surface, as can occur in dilute Ga solutions.[6]

Here, we use in situ transmission electron microscopy (TEM) to observe directly the formation of a crystalline 2D compound at the surface of liquid Au–Si. By varying both temperature and composition we find that the 2D phase can be stable over a surprisingly large range, over 150 °C, extending above and below the eutectic temperature. We develop a simple thermodynamic model that explains the wide stability range and composition dependence. Given the persistence of the surface ordering, we explore its effects on critical aspects of the behavior of Au–Si. We find that the surface layer plays a key role in the pathway of eutectic decomposition of Au–Si into solid Au + solid Si on cooling, and also that it is the root cause of the dramatic changes observed in the catalytic properties of Au–Si on cooling. We derive a strategy for controlling the presence of the surface phase as a tool in nanostructure fabrication.

Surface ordering on droplets of Au–Si of different diameters is shown in **Figure 1**a,b and Movie S1 in the Supporting Information. These high spatial and temporal resolution data (see the Supporting Information) were recorded by in situ heating of Si substrates decorated with Au nanoparticles, with or without exposure to the Si source gas disilane (Si_2H_6). On reaching the Au–Si eutectic temperature $T_E = 363$ °C,[12] the Au reacts with Si to form Au–Si liquid droplets. Imaging the surfaces of these droplets in profile view (Figure 1a) shows that there are two well-defined crystalline layers at the surface. The ordering can also be detected in projection over the entire droplet area in Figure 1a. In the smaller droplet shown

Dr. F. Panciera,[+] Prof. S. Hofmann
Department of Engineering
University of Cambridge
9 J. J. Thomson Avenue, Cambridge CB3 0FA, UK
E-mail: federico.panciera@c2n.upsaclay.fr
Dr. F. Panciera, Dr. J. Tersoff, Dr. M. C. Reuter, Dr. F. M. Ross[++]
IBM T. J. Watson Research Center
Yorktown Heights, NY 10598, USA
E-mail: fmross@mit.edu
Dr. A. D. Gamalski, Dr. D. Zakharov, Dr. E. A. Stach
Center for Functional Nanomaterials
Brookhaven National Laboratory
Upton, NY 11973, USA

(iD) The ORCID identification number(s) for the author(s) of this article can be found under https://doi.org/10.1002/adma.201806544.

[+]Present address: Centre de Nanosciences et de Nanotechnologies, CNRS, Université Paris-Sud, Université Paris-Saclay, Avenue de la Vauve, 91120 Palaiseau, France
[++]Present address: Department of Materials Science and Engineering, Massachusetts Institute of Technology, 77 Massachusetts Avenue, Cambridge, MA 02139, USA

ADVANCED
SCIENCE NEWS
www.advancedsciencenews.com

ADVANCED
MATERIALS
www.advmat.de
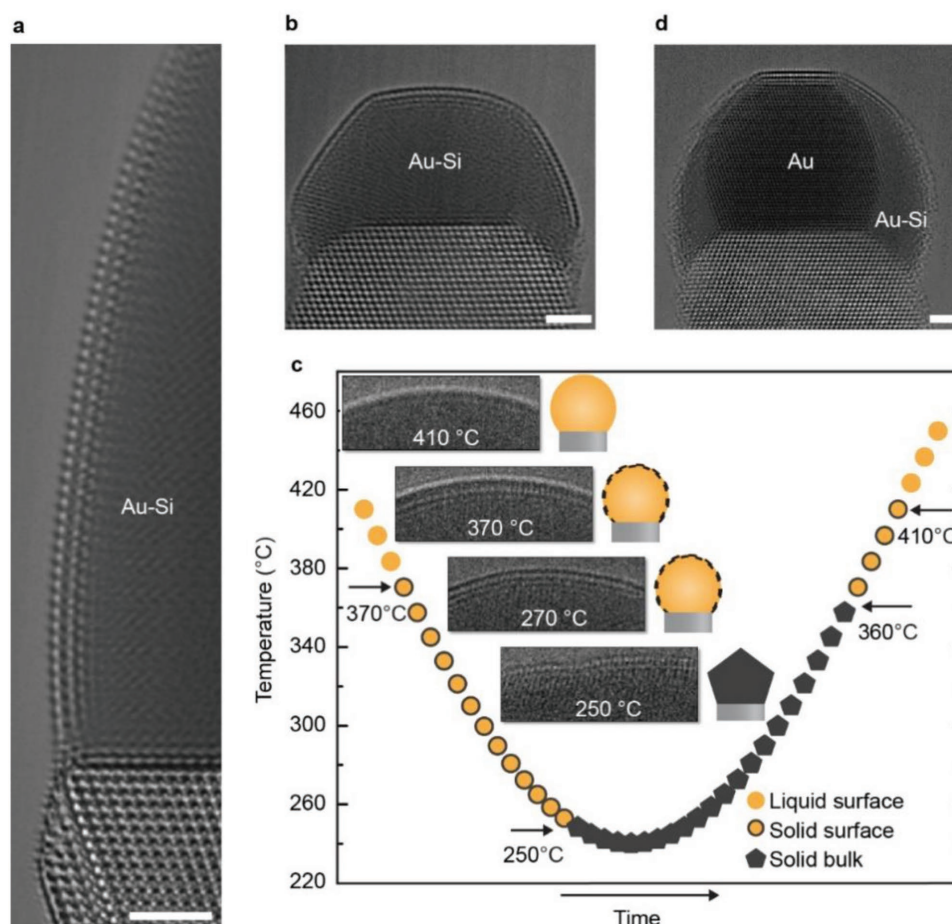
Figure 1. Crystalline ordering at the surface of Au–Si liquid. a) The 2D surface phase on a 50 nm diameter droplet at 350 °C visualized by adding aberration-corrected subimages aligned to remove effects of drift. A crystalline bilayer is visible with interlayer spacing 0.35 nm (Table S1, Supporting Information). The contrast visible over the entire liquid droplet is assumed to be a projection of ordering present on top and bottom surfaces. b) Surface ordering on a smaller 12 nm diameter droplet at 350 °C. Several 2D domains are visible separated by high-curvature boundaries. Thermal motion of the structure is shown in Movie S1 in the Supporting Information. c) Schematic summary of the evolution during cooling and heating, with insets showing one particular droplet during cooling. d) Image obtained during heating of a solid Au particle on Si. At the time shown, T = 360 °C and the Au has partially reacted with Si so that eutectic liquid covers part of its surface. Ordering is visible both on the liquid surface and on the (111) surface of the remaining solid Au. All scale bars are 2 nm.

in Figure 1b, bending rigidity of the surface phase is evident: the droplet is deformed into a polyhedron bounded by relatively flat "facets," having radius of curvature 80–100 nm, that meet at higher angle edges. The facets and edges undergo dynamic motion at the measurement temperature, shown in Movie S1 in the Supporting Information. To eliminate effects of surface oxidation or other extraneous reactions that may arise from the microscope background vacuum (relatively poor at 10^{-6} Torr), identical experiments were carried out in a TEM with an ultrahigh vacuum (UHV) sample environment (2×10^{-10} Torr). In this instrument, we identify surface ordering under equivalent conditions via the faceting of otherwise liquid droplets, even though the atomic level details at the surface are not resolved.

We evaluate the presence and structure of the surface phase as a function of temperature by heating and cooling droplets on a Si substrate. A cooling and reheating cycle is shown schematically in Figure 1c. The droplet exhibits supercooling, remaining in a liquid state well below T_E; at ≈250 °C Au and Si rapidly

separate and solidify; then liquid reappears as T_E is reached. The surface ordering shows distinctive behavior. On cooling, it consistently appears at ≈370 °C and remains visible until solidification. On heating, it becomes visible as soon as liquid starts to appear at T_E (Figure 1d) and it persists up to 410 °C. The pronounced temperature hysteresis suggests a first order phase transition at 410 °C, with supercooling to 370 °C before the ordered phase appears.

A striking feature of the ordered surface layer in Figure 1c is that its structure and thickness appear constant over its range of stability, with no other phase visible. We also find that a structure with similar lattice parameters is present on the surface of solid Au at temperatures where ordering is present on the liquid (Figure 1d, with more detail in Figure S1, Supporting Information). The lattice spacing, number of crystalline layers, and stiffness of the ordered surface layer correspond to the LT surface phase previously identified[2] in diffraction (Table S1, Supporting Information), and the bending rigidity is also consistent with the LT phase.[8,2] However, in our experiments the
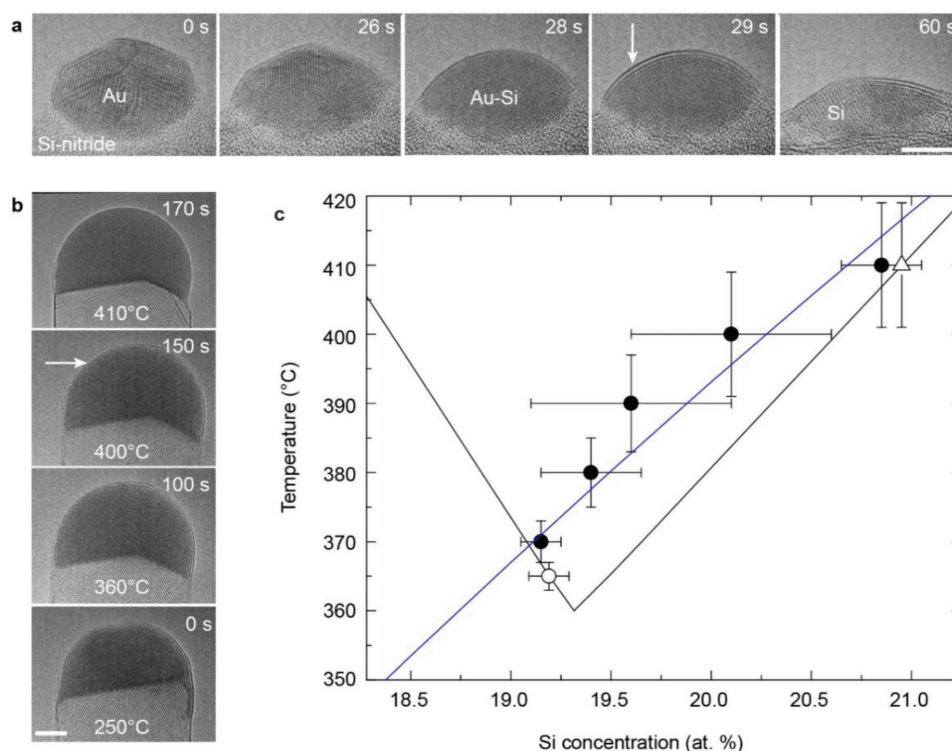
Figure 2. Surface ordered phase versus temperature and composition of liquid Au–Si. Solid arrows indicate the formation of the ordered 2D phase. All scale bars are 5 nm. a) Au nanoparticles on SiN exposed to Si_2H_6 (1.5×10^{-5} Torr) at 370 °C. The ordered phase appears just after complete reaction of solid Au. b) Si nanowire heated in vacuum. The solid to liquid Au–Si transition and the 2D phase appear at 360 °C (i.e., the expected eutectic temperature); the 2D phase disappears at 410 °C. c) Au–Si phase diagram near the eutectic point. Solid circles, from the complete data set in Figure S2 in the Supporting Information, show the liquid composition at which the 2D phase appears during isothermal addition of Si. The open circle shows a temperature at which the 2D phase is already visible as soon as liquid appears, indicating that this point lies below the phase boundary. The open triangle shows disappearance of order during heating in equilibrium with Si. The blue line shows the calculated phase boundary for the melt/freeze transition of the solid surface layer using a value of $\Delta \Gamma_s = -0.037$ J m^{-2} obtained by fitting to the solid circle data points.

surface ordering is stable up to 410 °C, much higher than the stability up to 371 °C reported for LT.[2]

To understand the driving force that forms the surface ordering, and its unexpected stability, we first note, as above, that our system is not exhibiting classic prefreezing,[11] since the surface phase does not change its thickness even over a range of 150 °C. On the other hand, its formation cannot be explained using bulk thermodynamic arguments since Au–Si solid compounds are not present on the phase diagram. To develop a model that explains the observations we therefore probe in more detail the conditions under which the surface phase is stable on liquid Au–Si, addressing the dependence on both composition and temperature.

We first explore the formation of the surface phase as a function of composition (**Figure 2**a). This was achieved by placing Au nanocrystals on an inert support (see the Experimental Section), heating to a fixed temperature, then gradually adding Si by flowing the source gas disilane (Si_2H_6). As expected from the phase diagram,[12] above T_E the Au is progressively converted to Au–Si liquid. Further addition of Si enriches the liquid in Si, eventually nucleating solid Si (Movie S2, Supporting Information). During this sequence, the presence of surface ordering can be evaluated. At 410 °C, surface ordering is not present on the Au–Si when it forms initially but appears as the Au–Si composition approaches the Si liquidus line (i.e., shortly before Si

nucleation). At lower temperatures, surface ordering becomes visible closer to the Au liquidus line (Figure S2, Supporting Information). At 370 °C or below, surface ordering is visible as soon as any liquid forms, i.e., at the Au liquidus composition. This is shown on the phase diagram in Figure 2c. The transition temperature between ordered and disordered surfaces increases sharply with Si composition. To evaluate the stability of surface ordering as a function of temperature, we examine Au–Si droplets that are in contact with Si (Figure 2b). As the temperature varies, the presence of the Si reservoir fixes the Au–Si at the liquidus composition. Ordering is visible between T_E and 410 °C. This stability range is consistent with Figure 1b and is shown as a triangle on the phase diagram in Figure 2c.

To model the phase boundary between the ordered and disordered liquid surface, we consider the 2D surface phase to be a surface reconstruction of the liquid. We then calculate the transition as we would the transition between two reconstructions of a solid surface, via minimization of the surface free energy. We assume that the structure and composition of the 2D solid are fixed and correspond to that reported for the LT phase (Au_4Si_8).[2] For simplicity we neglect all nonessential effects, including finite size effects as well as any variation of the liquid–vapor and liquid–solid interfacial free energies or of the net interfacial segregation in the liquid with composition and temperature. With these approximations, we can write the

**ADVANCED
SCIENCE NEWS**
www.advancedsciencenews.com

**ADVANCED
MATERIALS**
www.advmat.de

free energy change ΔF_s upon forming an ordered surface layer as

$$\Delta F_s = \Delta \Gamma_s - N_{Au}\mu_{Au} - N_{Si}\mu_{Si} \tag{1}$$

where the solid has areal density N_{Au} and N_{Si} of Au and Si atoms, respectively, and the μ's are the chemical potentials of these atoms in the liquid. It is convenient to take elemental solid Au and Si as reference states, so $\Delta\Gamma_s$ is the change in free energy upon taking $N_{Au} + N_{Si}$ atoms from the reference solids and assembling them as a 2D crystal on the liquid surface. Since the surface phase corresponds well with the LT phase, we use the N values given in ref. [2] and μ_{Au} and μ_{Si} are calculated using a standard thermodynamic model.[13] We neglect the entropic component of $\Delta\Gamma_s$, treating $\Delta\Gamma_s$ as independent of T, since (by our choice of reference) it involves no change in the number of liquid atoms. Thus, there is only one unknown parameter in the model, $\Delta\Gamma_s$.

We find we can reproduce the experimental results (Figure 2c and Figure S3, Supporting Information) to within their error bars by an appropriate choice of $\Delta\Gamma_s$. In particular, the calculated slope matches the measured one with no adjustable parameters, since to a good approximation changing $\Delta\Gamma_s$ simply shifts the boundary up and down in temperature. The best fit with the experimental data is obtained for $\Delta\Gamma_s = -0.037$ j m^{-2}. This is a tiny value, only 7% of the surface tension of Au–Si,[14] the key being simply that it is negative, rather than positive as in other systems. Thus, the existence of the surface phase can be explained simply by the solid phase having an unusually low surface energy, relative to the liquid. The model directly explains the surprisingly large range of stability observed: because the solid phase is Si-rich, its free energy decreases as the liquid becomes more Si-rich, stabilizing the phase to higher temperatures.

We find that the surface ordering plays a crucial role in the eutectic decomposition of liquid Au–Si into solid Au + solid Si on cooling. With experiments at high spatial and temporal resolution, we find that there are two steps in this process (Figure S4 and S5 and Movie S3, Supporting Information). The liquid first solidifies into a metastable Au–Si crystalline phase, then this phase decomposes into crystalline Au and Si. Remarkably, the ordered surface layer appears unchanged throughout, and the metastable phase grows from the ordered surface layer inward and inherits the orientation of the surface phase (Figure S5, Supporting Information). It is interesting that the surface phase survives even after the system decomposes into solid Au + Si (Figure S6, Supporting Information).

Various metastable Au–Si phases are known to form as intermediate states during rapid quenching of Au–Si liquid.[12,15] The metastable phase observed in Figure S5 in the Supporting Information is consistent with one of these phases, δ_1 (Supporting Information). We suggest that its good match with the surface phase can explain why δ_1, out of the many known metastable Au–Si solid phases,[12,16] is preferentially observed during cooling of nanoscale droplets where surface effects are dominant, while other metastable phases are more commonly found at the macroscale.[17] Our nanoscale droplets can be considerably supercooled (as in Figure 1a), indicating a substantial energy barrier to forming a solid.[18] When crystallization does

take place, we see it starting at the surface. The ordered surface phase appears to act as a template for δ_1, making this the crystallization pathway with lowest free energy barrier. In fact, we can consider the surface phase as a surface reconstruction of the δ_1 phase, as it persists at the surface of δ_1 after solidification.

We next consider how the surface ordering affects the catalytic properties of liquid Au–Si. Au–Si droplets are the first and most widely used catalysts for nanowire growth.[19,20] On supplying Si to a Au–Si droplet, the liquid becomes supersaturated with Si which then precipitates at the droplet/substrate interface to form a nanowire. In **Figure 3**, we show that the presence of surface ordering radically changes the ability of the droplet to catalyze this growth process. At constant Si flux (controlled via disilane pressure), nanowire growth decreases abruptly as the temperature is lowered. The dramatic change in growth rate correlates with formation of the surface phase (Figure 3b,c and Movie S4, Supporting Information). The nanowire growth stops within our measurement capability, although we do not exclude the possibility that the wire is still growing at a very low rate, since slow growth has been observed near T_E[21] under conditions where the rate at higher temperature is 30× our value.

This connection between growth rate and surface ordering solves the longstanding puzzle of why Si nanowires cannot be grown below the eutectic temperature, while Ge and alloy Si-Ge nanowires can grow far below T_E from the supercooled liquid.[22–24] For Si, the catalytic activity of the liquid surface is quenched when the ordering appears. The behavior is consistent with observations that liquid surfaces are generally more reactive than crystalline surfaces in catalysis of gases,[25] and also that nanowire growth from completely solid catalysts such as solid Au[26] or AuAg[27] is very slow compared with liquid catalysts. Nanowire growth involves several steps: sticking and dissociation at the catalyst surface, diffusion through the catalyst, and addition of crystal layers at the liquid/nanowire interface. The present observation implies that the liquid surface has either a higher sticking probability or a higher efficiency in dissociating the precursor molecules than the ordered surface. From the present data, we cannot separate these two causes. However, we expect that the state of the interior of the catalyst (i.e., solid or liquid) is not likely to play a role since diffusion through either solid or liquid is not rate limiting in nanowire growth.[28] In contrast to Au–Si, Au–Ge does not form a crystalline surface phase,[29] so its catalytic properties should be preserved at lower temperatures. Low temperature is in fact commonly used for Ge nanowire growth as the morphology is improved by reduced sidewall deposition.[27,30,31]

To test the relationship between surface ordering and catalytic properties, we examined catalysis by droplets exposed to Si and Ge at constant temperature. In Figure 3d and Movie S5 in the Supporting Information, we show that the ordered surface phase disappears after adding about one monolayer of Ge to the droplet, allowing growth below T_E. Ge and AuGe have lower surface energy than Si and AuSi respectively, so we expect Ge to segregate to the surface. Because our model shows that the stability of the Au–Si ordered phase is caused by its slightly lower surface energy compared to the liquid phase, even a small reduction in liquid surface energy by Ge would be sufficient to destabilize it. On reintroducing pure Si_2H_6, the surface phase eventually reappears and growth stops (see the Supporting
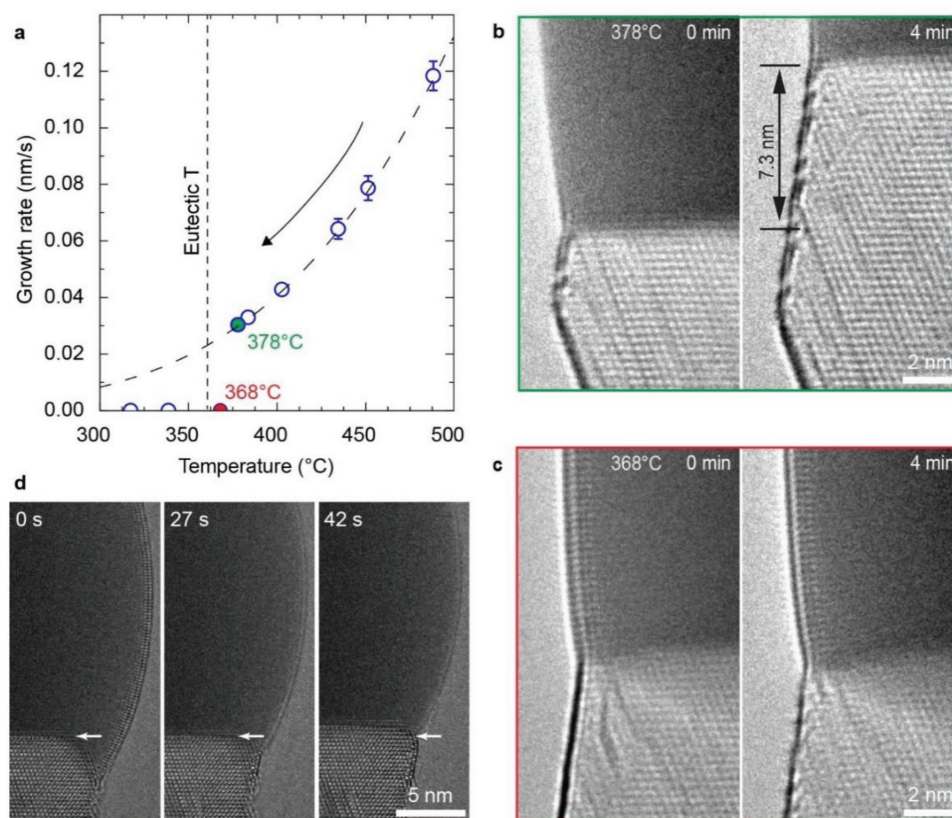
Figure 3. Impact of the surface phase on catalytic properties. a) Growth rate versus temperature during cooling, for a Si nanowire growing in 1×10^{-5} Torr Si_2H_6. The error in T is ± 10 °C. The error bar on the growth rate is calculated assuming uncertainties in measurement of length 1 nm and time 0.05 s. For each temperature, growth of a segment of ≈15 nm was timed; lower T required more time, giving smaller error. The growth rate decreases smoothly with decreasing T, as expected,[35] until a break at ≈375 °C below which no measurable growth was observed after 45 min. b) Images at 378 °C at the times indicated, showing growth (at 0.03 nm s^{-1}) and no order at the droplet surface. Data correspond to the green circle in (a). c) Images at 368 °C showing no growth and the presence of the surface ordered layer. Data correspond to the red circle in (a). The full data set is shown in Movie S4 in the Supporting Information. d) Images recorded at 350 °C showing ordered surface in the absence of precursor gases; ordering disappears after 27 s exposure to 2×10^{-5} Torr Ge_2H_6; after 42 s, growth restarted to form a segment of SiGe (arrowed).

Information). This suggests a strategy for sub-T_E growth of nearly pure Si nanowires, which is to add a tiny fraction of Ge precursor to the Si source gas (see the Supporting Information). A trace amount of Ge would be incorporated in the nanowire, but most properties would not be noticeably affected. Accessing low temperature would improve aspects of Si nanowire growth such as the sharpness of axial p/n junctions by reducing the solubility of dopants in the droplet. Indeed, the surface phase can be considered as a growth tool: for example, changing the source gas conditions to create surface ordering would allow growth to be stopped without changing the pressure, which is known to destabilize droplets.[32]

The existence of the ordered surface phase on Au–Si over a range of conditions, and its role in the eutectic solidification pathway and effect on catalytic properties for Si nanowire growth, form a striking example of the unexpected phenomena that can occur at the surfaces of liquid metals. Liquid metals are well studied materials, yet there remain basic properties of their surfaces that can only be probed by controlled environment microscopy with good temporal and spatial resolution. The recent emergence of liquid metals as a new class of catalysts for the synthesis of graphene and other 2D materials[33] and 2D oxides[34] and for the catalytic conversion of gases[25] suggests that the study of surface phenomena in other liquid metals will be important in developing a deeper understanding and control of the properties of these materials.

Experimental Section

Sample Preparation and Imaging: The formation of Au–Si surface phases was observed in situ and with time resolution using two electron microscopes with complementary capabilities.

1) A Hitachi H-9000 ultrahigh vacuum TEM (UHV-TEM) was used to form Au–Si eutectic droplets and measure their surface structure and catalytic properties in the absence of effects due to background species in the microscope environment (water and oxygen). The instrument base pressure is 2×10^{-10} Torr and the maximum pressure during imaging is 2×10^{-5} Torr. This microscope is connected to a cluster of UHV tools where metal deposition was carried out. The substrates used were 3 mm × 300 µm silicon strips cut from a 700 µm thick (111) wafer. Each sample was loaded into the TEM loadlock, where it was baked at 100–150 °C under a tungsten lamp for 8 h to degas and remove moisture. It was then transferred to a UHV chamber and heated resistively by direct current up to 1200 °C for short pulses in order to desorb the native oxide and form flat Si terraces. At the same time, a

temperature versus heating current curve was measured by using a pyrometer to observe the sample through a viewport. The sample was then transferred under vacuum to a Knudsen cell Au evaporation system, thus maintaining an oxide-free surface. About 1 nm Au was deposited onto the {111} surface. The sample was finally transferred under vacuum to the TEM where precursor gas (Si_2H_6) was introduced through a capillary tube and the temperature was raised to 500 °C, again using direct current heating. This agglomerates Au into droplets and initiates Si adsorption and nanowire growth. Typical nanowire growth rates were in the range 5–15 nm min^{-1} at temperatures of 470–520 °C. The presence of the surface ordering (visible as facets on otherwise amorphous droplets) and the nanowire growth rate as a function of temperature were accurately determined from such in situ observations. For accurate temperature measurement, the temperature versus heating current curve was calibrated by identifying the current flowing at the eutectic point, using slow ramping upwards through the eutectic transformation.

2) An aberration-corrected FEI Titan 300 environmental TEM (ETEM) with capabilities to introduce group IV gas precursors and also equipped with a Gatan K2 fast camera (400 images s^{-1}) was used to provide high spatial and temporal resolution of structural changes of the Au–Si surface and bulk phases. Samples on which nanowires had been pregrown in the UHV-TEM were carried through air then loaded into the ETEM. A shell of SiO_2 was visible around the nanowires but this could be removed by condensing the intense electron beam spot around the catalyst droplet while holding the sample at 500 °C. Growth of wires and formation and destruction of surface ordering were obtained by flowing Si_2H_6 and Ge_2H_6. Separately, isothermal experiments were performed on Au aerosol particles on nitride-coated Si samples (3 mm × 300 µm silicon strips cut from a 700 µm thick (111) wafer). For these samples, 5 and 10 nm Au aerosol nanoparticles were deposited directly on the nitride layer. Samples were mounted in a conventional heating holder (Gatan) and imaged with the nitride-coated surface parallel to the beam. This heating holder uses current flow through a furnace surrounding the sample, measuring temperature via a thermocouple attached to the furnace. It was checked that the solid–liquid transition happened at the same temperature in the UHV-TEM calibrated with the pyrometer and in the ETEM as indicated by the thermocouple. The maximum gas pressures used were low ($2 × 10^{-5}$ Torr) and did not affect the substrate temperature. Any cooling effect due to the introduction of the gas would result in a drift of the sample, which was not observed. Cooling from the gas in ETEM is generally not visible below the $1 × 10^{-3}$ Torr range.

This procedure allowed direct observation in the ETEM of formation of the surface phase while changing the Au–Si composition at a given temperature. Experiments were repeated to verify that the formation of the surface phase occurred at the same temperature and composition over several regions of the sample. It was also verified that there was no visible difference between particles constantly exposed to the electron beam and particles observed sporadically.

Model for Thermodynamics of Surface Ordering: The N values used in the model are taken from ref. [2], $N_{Au} = 9.6 × 10^{-6}$ and $N_{Si} = 19.2 × 10^{-6}$ mol m^{-2} for one monolayer. Since the observations and ref. [8] show that the surface phase actually contains two monolayers, these values were doubled for the calculations. It is important to note that doubling the N values does not change the fitted curve, it simply doubles the value of the fitting parameter $\Delta\Gamma_s$. In particular, the slope of the curve is unaffected. Thus, the conclusions are the same whether a single or a double layer is modeled.

Supporting Information

Supporting Information is available from the Wiley Online Library or from the author.

Data Availability

Raw data are available upon request to the corresponding authors.

Conflict of Interest

The authors declare no conflict of interest.

[1] A. Turchanin, W. Freyland, D. Nattland, *Phys. Chem. Chem. Phys.* **2002**, 4, 647.
[2] O. G. Shpyrko, R. Streitel, V. S. Balagurusamy, A. Y. Grigoriev, M. Deutsch, B. M. Ocko, M. Meron, B. Lin, P. S. Pershan, *Science* **2006**, 313, 77.
[3] M. J. Regan, E. H. Kawamoto, S. Lee, P. S. Pershan, N. Maskil, M. Deutsch, O. M. Magnussen, B. M. Ocko, L. E. Berman, *Phys. Rev. Lett.* **1995**, 75, 2498.
[4] O. M. Magnussen, B. M. Ocko, M. J. Regan, K. Penanen, P. S. Pershan, M. Deutsch, *Phys. Rev. Lett.* **1995**, 74, 4444.
[5] B. Yang, D. Gidalevitz, D. Li, Z. Huang, S. A. Rice, *Proc. Natl. Acad. Sci. USA* **1999**, 96, 13009.
[6] C. Calmes, D. Giuranno, D. Chatain, *J. Mater. Sci.* **2009**, 44, 5949.
[7] B. Yang, D. Li, S. A. Rice, *Phys. Rev. B* **2003**, 67, 212103.
[8] S. Mechler, P. S. Pershan, E. Yahel, S. E. Stoltz, O. G. Shpyrko, B. Lin, M. Meron, S. Sellner, *Phys. Rev. Lett.* **2010**, 105, 186101.
[9] O. G. Shpyrko, R. Streitel, V. S. Balagurusamy, A. Y. Grigoriev, M. Deutsch, B. M. Ocko, M. Meron, B. Lin, P. S. Pershan, *Phys. Rev. B* **2007**, 76, 245436.
[10] A. L. Pinardi, S. J. Leake, R. Felici, I. K. Robinson, *Phys. Rev. B* **2009**, 79, 045416.
[11] B. Pluis, D. Frenkel, *Surf. Sci.* **1990**, 239, 282.
[12] H. Okamoto, T. B. Massalski, *Bull. Alloy Phase Diagrams* **1983**, 4, 190.
[13] P. Y. Chevalier, *Thermochim. Acta* **1989**, 141, 217.
[14] F. Panciera, M. M. Norton, S. B. Alam, S. Hofmann, K. Mølhave, F. M. Ross, *Nat. Commun.* **2016**, 7, 12271.
[15] M. Zhang, J. G. Wen, M. Y. Efremov, E. A. Olson, Z. S. Zhang, L. Hu, L. P. de la Rama, R. Kummamuru, K. L. Kavanagh, Z. Ma, L. H. Allen, *J. Appl. Phys.* **2012**, 111, 093516.
[16] L. Hultman, A. Robertsson, H. T. G. Hentzell, I. Engström, P. A. Psaras, *J. Appl. Phys.* **1987**, 62, 3647.

[17] H. S. Chen, D. Turnbull, *J. Appl. Phys.* **1967**, *38*, 3646.

[18] T. U. Schülli, R. Daudin, G. Renaud, A. Vaysset, O. Geaymond, A. Pasturel, *Nature* **2012**, *464*, 1174.

[19] R. S. Wagner, W. C. Ellis, *Appl. Phys. Lett.* **1964**, *4*, 89.

[20] V. Schmidt, J. V. Wittemann, U. Gosele, *Chem. Rev.* **2010**, *110*, 361.

[21] C. W. Pinion, D. J. Hill, J. D. Christesen, J. R. McBride, J. F. Cahoon, *J. Phys. Chem. Lett.* **2016**, *7*, 4236.

[22] S. A. Dayeh, J. Wang, N. Li, J. Y. Huang, A. V. Gin, S. T. Picraux, *Nano Lett.* **2011**, *11*, 4200.

[23] K. K. Lew, L. Pan, E. C. Dickey, J. M. Redwing, *Adv. Mater.* **2003**, *15*, 2073.

[24] K. K. Lew, L. Pan, E. C. Dickey, J. M. Redwing, *J. Mater. Res.* **2006**, *21*, 2876.

[25] N. Taccardi, M. Grabau, J. Debuschewitz, M. Distaso, M. Brandl, R. Hock, F. Maier, C. Papp, J. Erhard, C. Neiss, W. Peukert, *Nat. Chem.* **2017**, *9*, 862.

[26] S. R. Kodambaka, J. Tersoff, M. C. Reuter, F. M. Ross, *Science* **2007**, *316*, 729.

[27] Y. C. Chou, C. Y. Wen, M. C. Reuter, D. Su, E. A. Stach, F. M. Ross, *ACS Nano* **2012**, *6*, 6407.

[28] A. I. Persson, M. W. Larsson, S. Stenström, B. J. Ohlsson, L. Samuelson, L. R. Wallenberg, *Nat. Mater.* **2004**, *3*, 677.

[29] P. S. Pershan, S. E. Stoltz, S. Mechler, O. G. Shpyrko, A. Y. Grigoriev, V. S. K. Balagurusamy, B. H. Lin, M. Meron, *Phys. Rev. B* **2009** *80*, 125414.

[30] H. Adhikari, P. C. McIntyre, A. F. Marshall, C. E. Chidsey, *J. Appl. Phys.* **2007**, *102*, 094311.

[31] A. D. Gamalski, J. Tersoff, R. Sharma, C. Ducati, S. Hofmann, *Nano Lett.* **2010**, *10*, 2972.

[32] B. Tian, P. Xie, T. J. Kempa, D. C. Bell, C. M. Lieber, *Nat. Nanotechnol.* **2009**, *4*, 824.

[33] S. Y. Li, C. Lin, W. Zhao, J. Wu, Z. Wang, Y. Shen, D. M. Tang, J. Wang, Q. Zhang, H. Zhu, L. Chu, W. Zhao, C. Liu, Z. Sun, T. Taniguchi, M. Osada, W. Chen, Q. H. Xu, A. T. S. Wee, K. Suenaga, F. Ding, G. Eda, *Nat. Mater.* **2018**, *17*, 535.

[34] A. Zavabeti, J. Z. Ou, B. J. Carey, N. Syed, R. Orrell-Trigg, E. L. Mayes, C. Xu, O. Kavehei, A. P. O'Mullane, R. B. Kaner, K. Kalantar-zadeh, *Science* **2017**, *358*, 332.

[35] S. Kodambaka, J. Tersoff, M. C. Reuter, F. M. Ross, *Phys. Rev. Lett.* **2006**, *96*, 096105.